



Supplement of

Sources of surface O₃ in the UK: tagging O₃ within WRF-Chem

Johana Romero-Alvarez et al.

Correspondence to: Johana Romero-Alvarez (lero1992@colorado.edu)

The copyright of individual parts of the supplement might differ from the article licence.

S1. Model evaluation

S1.1 Meteorology

The meteorological dataset used in the model evaluation includes hourly observations of near ground air temperature (T) and wind speed and direction at 10 meters above the ground (WS and WD, respectively) at 21 sites using the land surface observational data UK's Met Office Integrated Data Archive System (MIDAS) (Met Office, 2006). The statistical analysis was performed using the R-Openair package (Carslaw and Ropkins, 2012) and statistical scores that include the mean bias (MB), the normalized mean bias (NMB), and the Pearson correlation coefficient (r). Table S1 lists the average statistical performance of modelled temperature and wind speed across UK.

Table S1. Average statistics for modelled temperature and wind speed performance, from May to August 2015, across the UK. The units of MB are the same as the observations.

Parameter	MB	NMB (%)	r	No sites
T (°C)	0.4	7	0.8	21
WS (m s ⁻¹)	-3.7	-39	0.4	6

The model represents well the observed near-surface air temperature and diurnal variability over the UK, as shown in Fig. S2, with correlation values ranging between 0.9 and 0.5 across the selected sites. The model is biased positively in most of the assessed sites. The largest warm bias (MB = 3.7°C) is obtained at Boxworth Cambridgeshire, and the cold biases (MB = -2.3 °C) is obtained at Holsome Devon. The values of MB in the temperature over the UK are consistent with that reported by Mar et al. (2016) in the June-July-August 2006 evaluation of WRF-Chem over Europe, where cold bias mostly concentrates over Northern Ireland and the North and the southwest UK. The simulation gives an average NMB of 7% for the period between May and August.

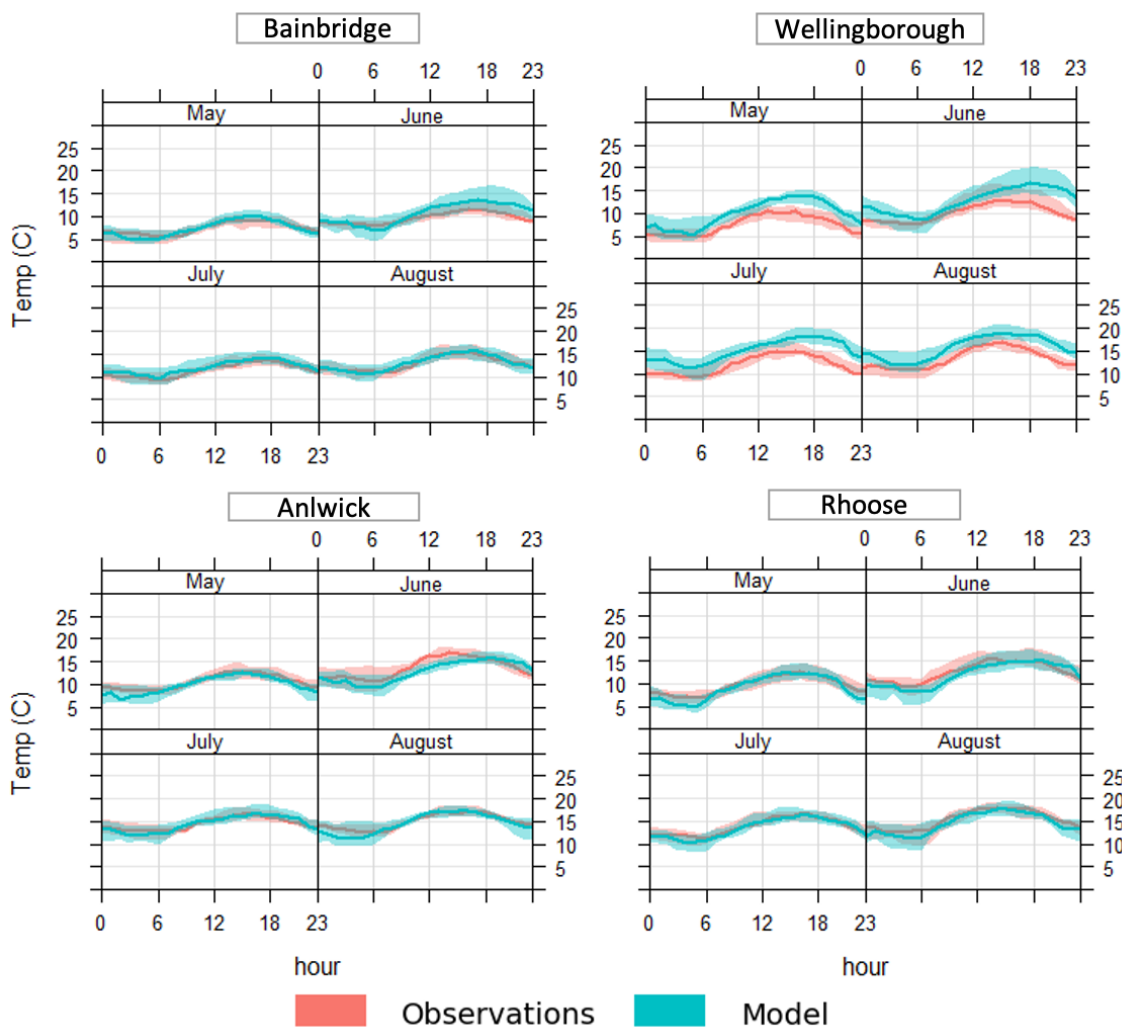


Figure S1. Comparison of the mean diurnal variation in temperature from May to August 2015 on selected sites in the UK.

Wind speed predictions exhibited inferior statistical performance. The average correlation coefficient is 0.4, with the lowest values showing no geographical preference. In particular, the model tends to predict moderate wind speed more frequently and fails to reproduce the highest observed wind speed values. Furthermore, the model is biased negatively in the majority of the sites with both the lowest biases ($MB = -5.3 \text{ ms}^{-1}$) and the highest biases ($MB = +0.9 \text{ ms}^{-1}$) obtained for the southwest. The MB values are closer to those reported by Zhang et al. (2013) in the model validation of WRF/Chem-MADRID and WRF/Polyphemus over Europe where wind speed is under-predicted at many sites in the UK (with MBs of -4 to -0.8 m s^{-1}). The simulation gives an average NMB of -39% for the period between May and August, which is in line with values reported in other application of the WRF-Chem model e.g., Gao et al. (2018) and Tao et al. (2020).

Comparison of modelled and observed wind speed direction. Fig. S2 shows that the sites are predominately positive bias (bias shown in polar coordinates) ranging between 3 and 23.7° North. The model does a better job simulating winds from south, southwest and southeast. The spread in the wind direction tends to be narrower across land sites in the midlands, such as Cirencester, Dagenham and Wilford Hill, when compared to those sites that are closer to the coast, e.g., Sibsey. The figure also shows that positive biases in wind speed tend to predominate during southerly, easterly, and westerly winds at most stations. In contrast, negative biases in wind speed are mostly associated with northerly winds. Hence, enhancement in horizontal advection of O_3 and precursors during anticyclonic weather is expected in our simulations.

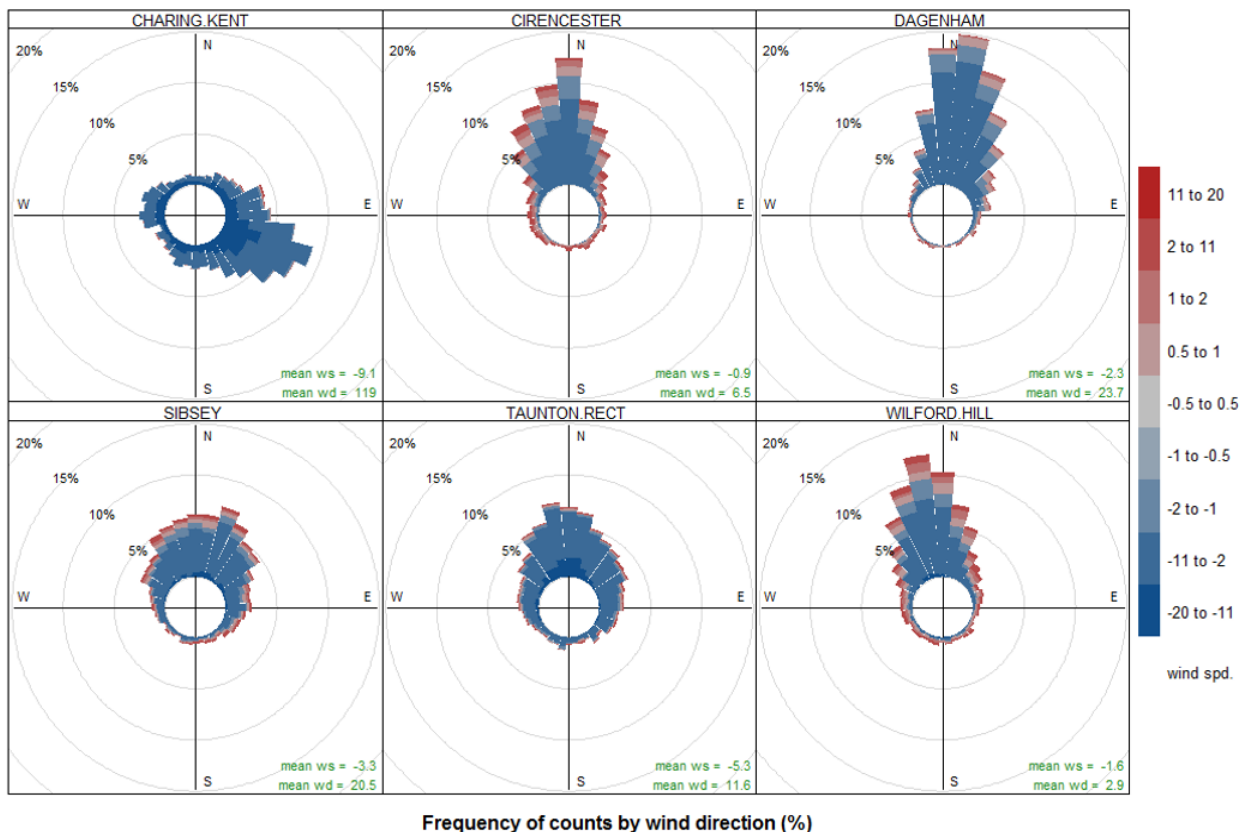


Figure S2. Bias between modelled and observed wind direction and speed, from May to August 2015, at six Met-office sites in the UK. Colors denote whether wind speed tend to be positively or negatively biased with respect to observations. Mean wind speed and direction bias are included as numerical values.

S1.2 Chemistry

Hourly surface O₃ measurements were taken from the European Monitoring and Evaluation Programme (EMEP) (<http://www.nilu.no/projects/ccc/>) from April to August 2015 at available sites in the UK, Ireland, France, The Netherlands, Switzerland, Denmark, Austria, and Germany. Surface measurements of NO and NO₂ were also taken for the same stations when available. Table S2. Sumarises the statistical performance.

Table S2. Statistics of hourly NO, NO₂ and O₃ calculated between May and August 2015. MB is given in ppbv.

Parameter	MB	NMB (%)	r	No sites
NO (ppbv)	-0.4	-39	0.3	15
NO ₂ (ppbv)	0.3	19	0.3	16
O ₃ (ppbv)	-3.7	6	0.6	52

Fig. S3 shows that the observed night-time mixing ratios typically remain above zero. In contrast, the modelled NO reach zero most of the time. The model struggles to capture the timing in diurnal NO peaks, with NO mixing ratios increasing earlier than observed. Negative NO biases at night may be attributed to errors in the reported night time NO observations due to high NO detection limits of the equipment relative to the real concentration levels at the site (Tørseth et al., 2012). On the other hand, the early peaks in daytime NO may be due to uncertainties in the emission inventory, particularly the diurnal pattern applied

to the emissions. Fig. S3 further shows that even though NO_2 diurnal variability is well captured at some sites, mixing ratios can be largely overestimated. As discussed in the main manuscript, positive bias in NO_2 , particularly at night, are expected in our simulations due to the omission of heterogeneous chemistry. An additional source of bias can be related to how the chemical mechanism represents the NO_x chemical cycles. A comparison of different chemical mechanisms reported in Knote et al. (2014) shows large overestimations of NO_x by the MOZART-4 mechanism and strong suppression of OH and HO_2 radicals caused by an incorrect rate constant for the reaction between NH_3 and OH.

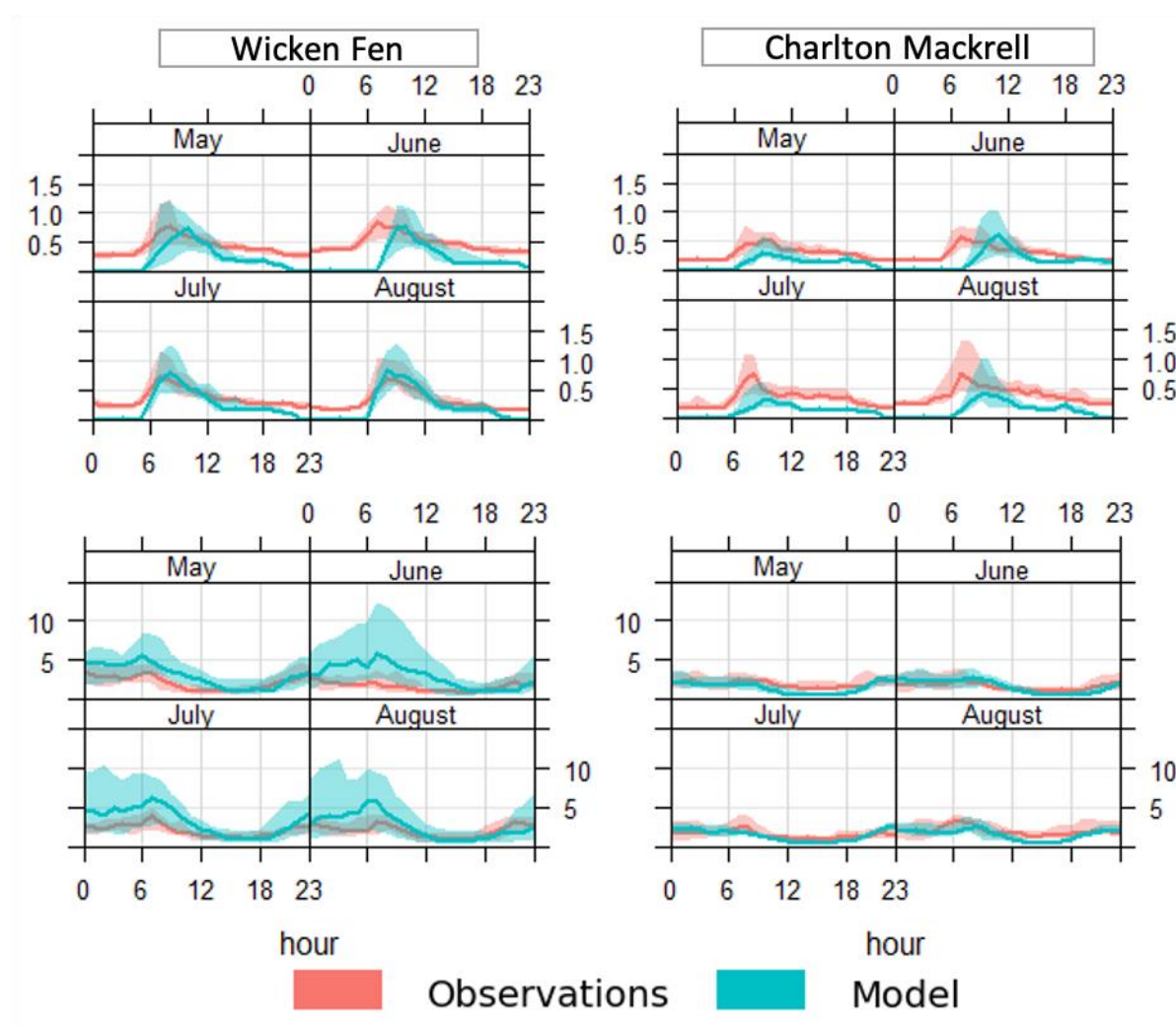


Figure S3. Mean diurnal variation in observed (red) and modelled (blue) NO and NO_2 mixing ratios at Wicken Fen and Charlton Mackrell. The shaded areas represent the variability between the different days, showing the 25th and 75th percentiles.

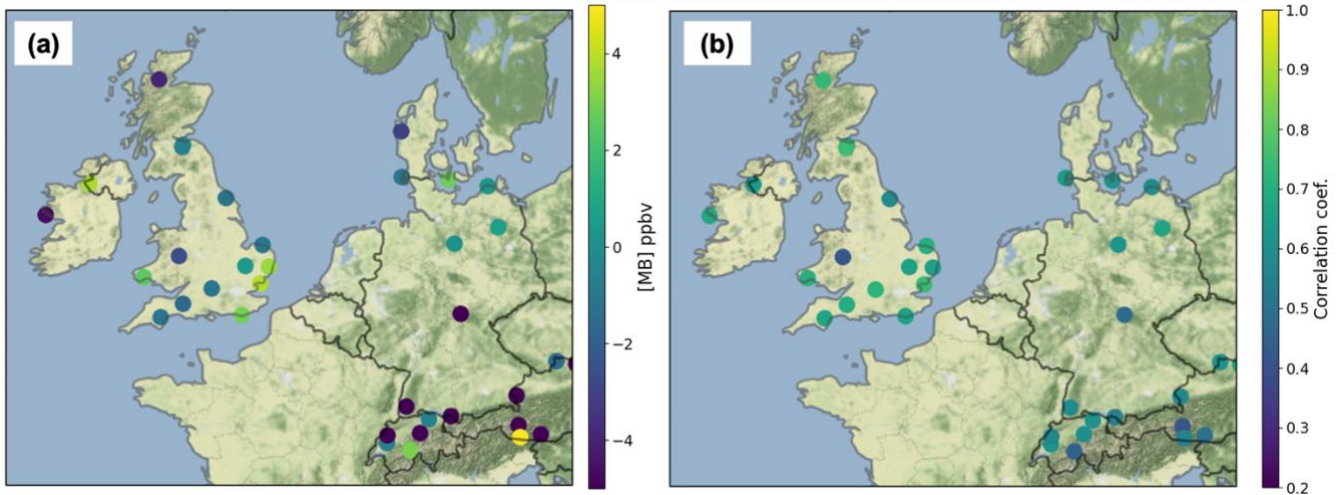


Figure S4. Mean bias MB ppbv (a) and correlation coefficient r (b) calculated from hourly measurements at each site.

Fig. S4 show that the modelled O_3 negative biases is up to -15 ppbv and positive MB of up to and + 5 ppbv. Negative biases are mostly restricted to sites in the North, and West of the UK and the throughout the Alps. Mace Head, for instance, exhibits a negative MB of -4.6 ppbv. Due to its geographical location on the western fringe of the UK, this site is strongly influenced by the model boundary conditions. Hence, the underestimations are most likely caused by biases in the representation of background O_3 entering the western fringe of the domain, particularly the O_3 predictions in the model used for boundary conditions (MOZART-4).

Fig. S5 shows that underestimations of O_3 in Mace Head are greatest during July and August. In contrast, underestimations of O_3 in sites such as Charlton Mackrell, Strathvaich, Weybourne, Auchencorth Moss and High Muffles, arise from the model having difficulties in capturing the diurnal changes in O_3 , and in particular day time concentrations during the summer months. Positive biases, on the other hand, are mostly observed in the east and southeast UK and north of Germany, with a few exceptions, see Fig. S5. Overestimated O_3 concentrations at Bush Estate, Narberth, Sibton and Wicken Fen, for instance, are due to the model struggling to reproduce the diurnal changes in O_3 , giving high O_3 concentrations during night-time, Fig. S5. This is consistent with insufficient titration of O_3 at night due to the underestimated NO discussed in the previous section. An additional source of model bias may be also caused by the limitation of comparing grid cell averages with point observations and by the choice of the grid cell representing each site

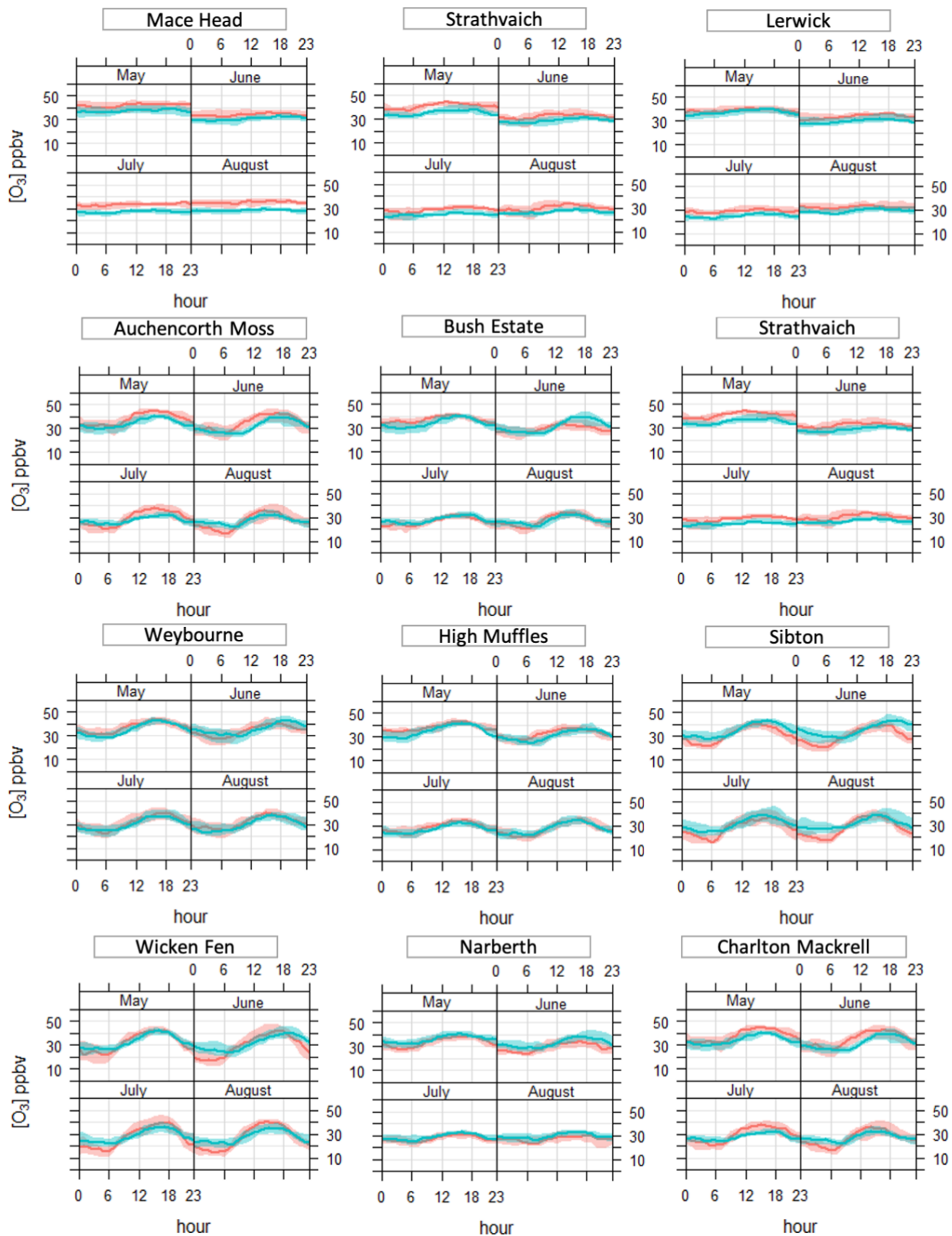


Figure S5. Diurnal variation in modelled and observed O_3 mixing ratios at selected sites in UK and the Republic of Ireland. The shaded areas represent the variability between the different days, showing the 25th and 75th percentiles.

Two additional metrics were considered for O_3 , the MDA8 O_3 , and the AOT40. The MDA8 O_3 was estimated by computing 8-h moving mean of O_3 , for both modeled and observations at each site, and by selecting the hours when the MDA8 of 50 and 60 ppbv was exceeded, following the current European and national air quality standards. The AOT40 was calculated by extracting the hours when O_3 mixing ratios exceeded the hourly 40 ppbv thresholds between 08:00 and 20:00 CET.

Fig. S6 shows the number of days with the MDA8 O_3 above 50 ppbv at 15 EMEP monitoring sites from May to August over the UK and the Republic of Ireland. The UK's Air quality strategy states that the MDA8 O_3 should not exceed the threshold value of 50 ppbv more than ten times a year. The figure shows that most of the observed concentrations at the stations had less than ten days above 50 ppbv apart from those located in the East Anglia region, southwest and southeast England. The largest MDA8 O_3 is seen at Wicken Fen, Yarner Wood, Weybourne, Sibton and Lullington Heath with 17, 15, 14, 12 and 12 days with MDA8 O_3 values above 50 ppbv respectively. Fig. S5 further shows that the model does a fair job capturing the spatial distribution of the MDA8 O_3 above 50 ppbv with the largest number of days concentrated in the East Anglia region and Southeast England. Nonetheless, the model tends to underestimate the number of days with MDA8 O_3 above 50 ppbv, in particular over the East Anglia region, which is in line with earlier studies stressing the poor performance of many air quality models in simulating peak O_3 concentrations in the UK (e.g., Archer-Nicholls et al., 2014; Francis et al., 2011).

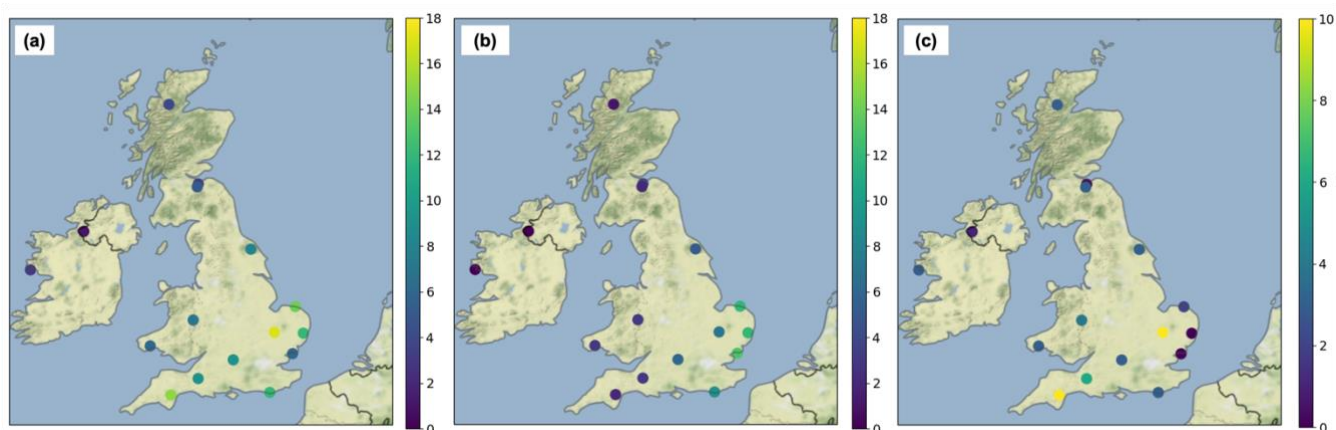


Figure S6. Spatial distribution of (a) observed and (b) modelled number of days with a daily MDA8 O_3 above 50 ppbv at EMEP monitoring sites calculated from May to September. The difference between observed and modelled MDA8 (observations – model) is also shown in (c). Please note the different scale used on (c).

The spatial distribution of the number of days with MDA8 O_3 above 60 ppbv is shown in Fig. S7. The European Union's Air Quality Directive long term objective states that the MDA8 O_3 should not exceed the threshold value of 60 ppbv within a calendar year. The observed values show that most of the sites have less than five days above 60 ppbv, except for some sites in the East of UK (East Anglia and the East Midlands). Similar to the MDA8 O_3 above 50 ppbv metrics, the model tends to underestimate the number of days with MDA8 O_3 above 60 ppbv in particular in the East Anglia Region. This is consistent with what has been reported for coarse simulations over a European domain for summertime using MOZART chemistry within WRF-Chem (Mar et al., 2016). Some overestimations of the metric, never higher than 5 days, are observed in the northeast UK.

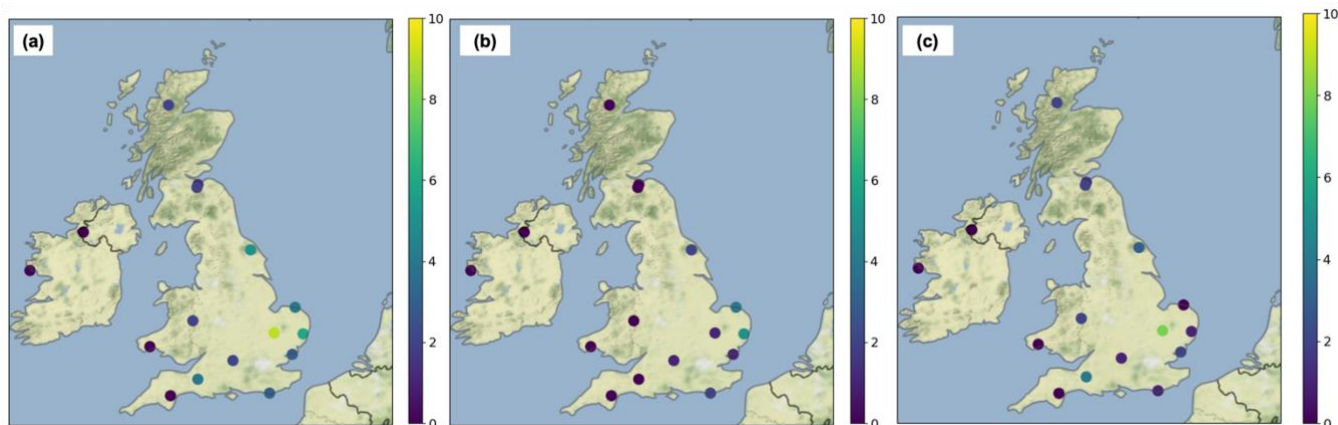


Figure S7. Spatial distribution of (a) observed and (b) modelled number of days with a daily MDA8 O₃ above 60 ppbv at EMEP monitoring sites calculated from May to September. The difference between observed and modelled MDA8 (observations – model) is also shown in (c).

The metric for vegetation exposure AOT40 is shown in Fig. S8. The UK’s Air Quality Directive states a target value of 9000 ppb h (~18000 $\mu\text{g m}^{-3}$ hours) averaged over five years. The highest observed values are seen in the east of England (with up to 6000 $\mu\text{g m}^{-3}$ hours observed at Weybourne and Wicken Fen) and the southwest. The model captures most of the spatial distribution of the AOT40, with the largest values obtained for East Anglia. However, it tends to underestimate observations in the southeast (up to - 3000 $\mu\text{g m}^{-3}$ hours), and overestimate them mostly in the southeast and Suffolk coast (e.g., St. Osyth up to 3000 $\mu\text{g m}^{-3}$ hours).

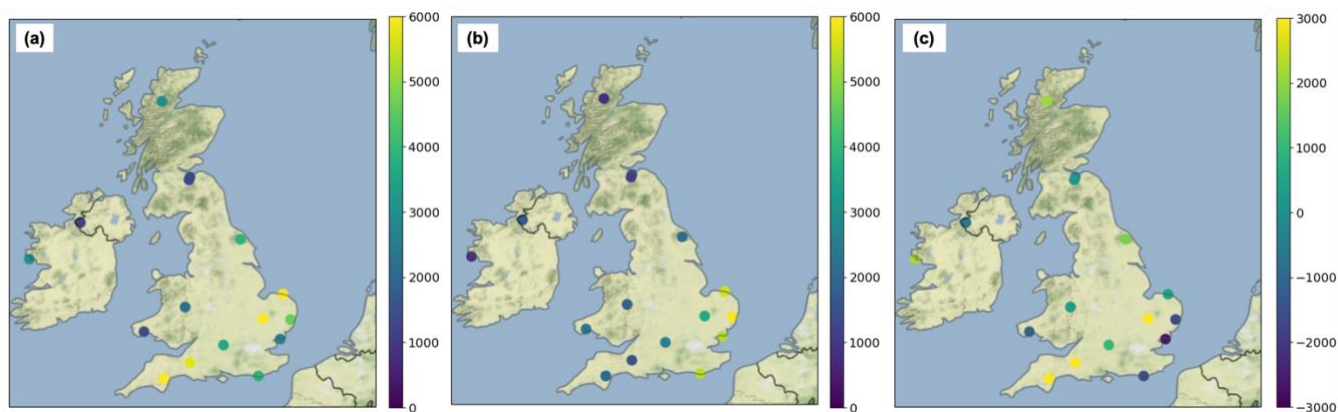


Figure S8. Spatial distribution of (a) observed and (b) modelled AOT40 ($\mu\text{g m}^{-3}$ hour) calculated from May to September. The difference between observed and modelled AOT40 (observations – model) is also shown in (c). Please note the different scale used on (c).

The model’s representation of organic NMVOCs may be an additional source of bias in the underestimation of O₃, particularly during days during MDA8 O₃ is above 50 and 60 ppbv. Figure S.9 shows that the model largely underestimates observations of isoprene particularly during the first days of July which were characterized by high O₃ mixing ratios. The impacts of isoprene chemistry in O₃ concentrations have been reported largely in the literature. For instance, in box modelling studies, Knote et al. (2014) show large variations in isoprene concentrations between different chemical mechanisms despite using identical biogenic emissions. Moreover, Zhao et al. (2016) demonstrate that more recent versions of the Model of Emissions of Gases

and Aerosols from Nature (MEGAN) better reproduce the observed isoprene than the publicly available version of the MEGAN model integrated into WRF-Chem

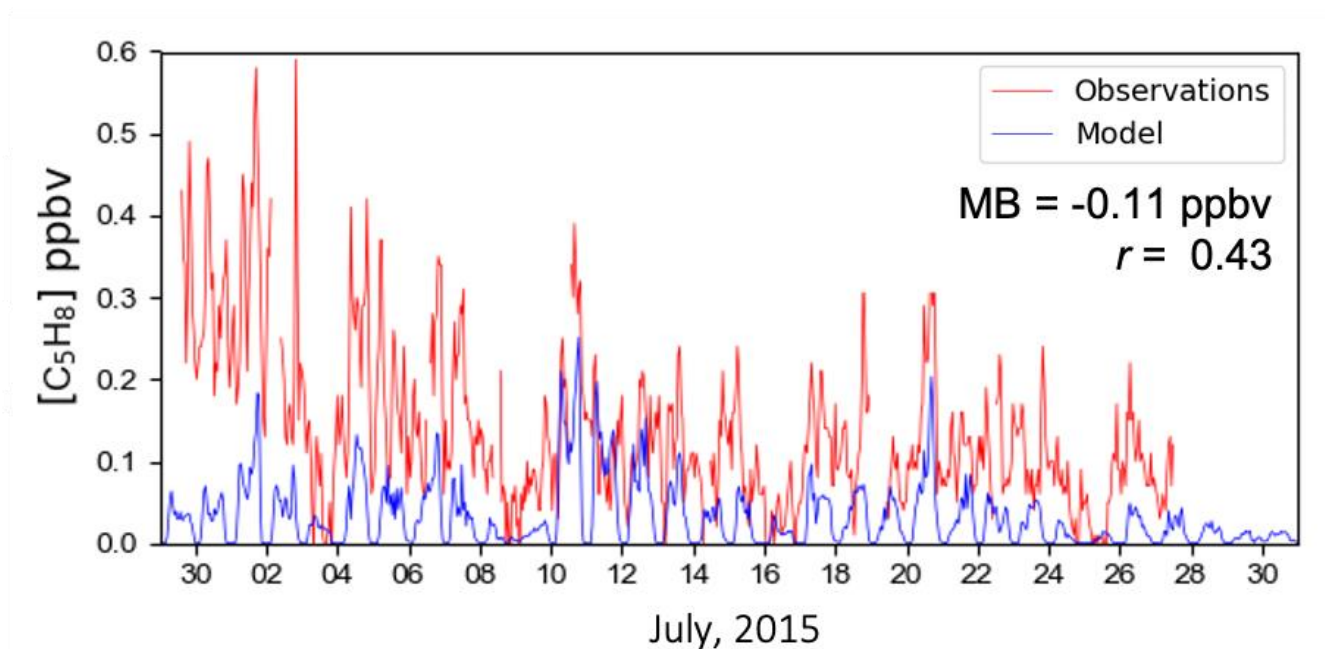


Figure S9. Comparison between modelled (blue) and observed (red) hourly isoprene mixing ratios at Weybourne Atmospheric Observatory on July 2015, East Anglia UK. Observational data obtained from the Integrated Chemistry of Ozone in the Atmosphere (ICOZA) field campaign, North Norfolk Coast, UK, summer of 2015 (Crilley et al., 2015).

S2. Regional contributions

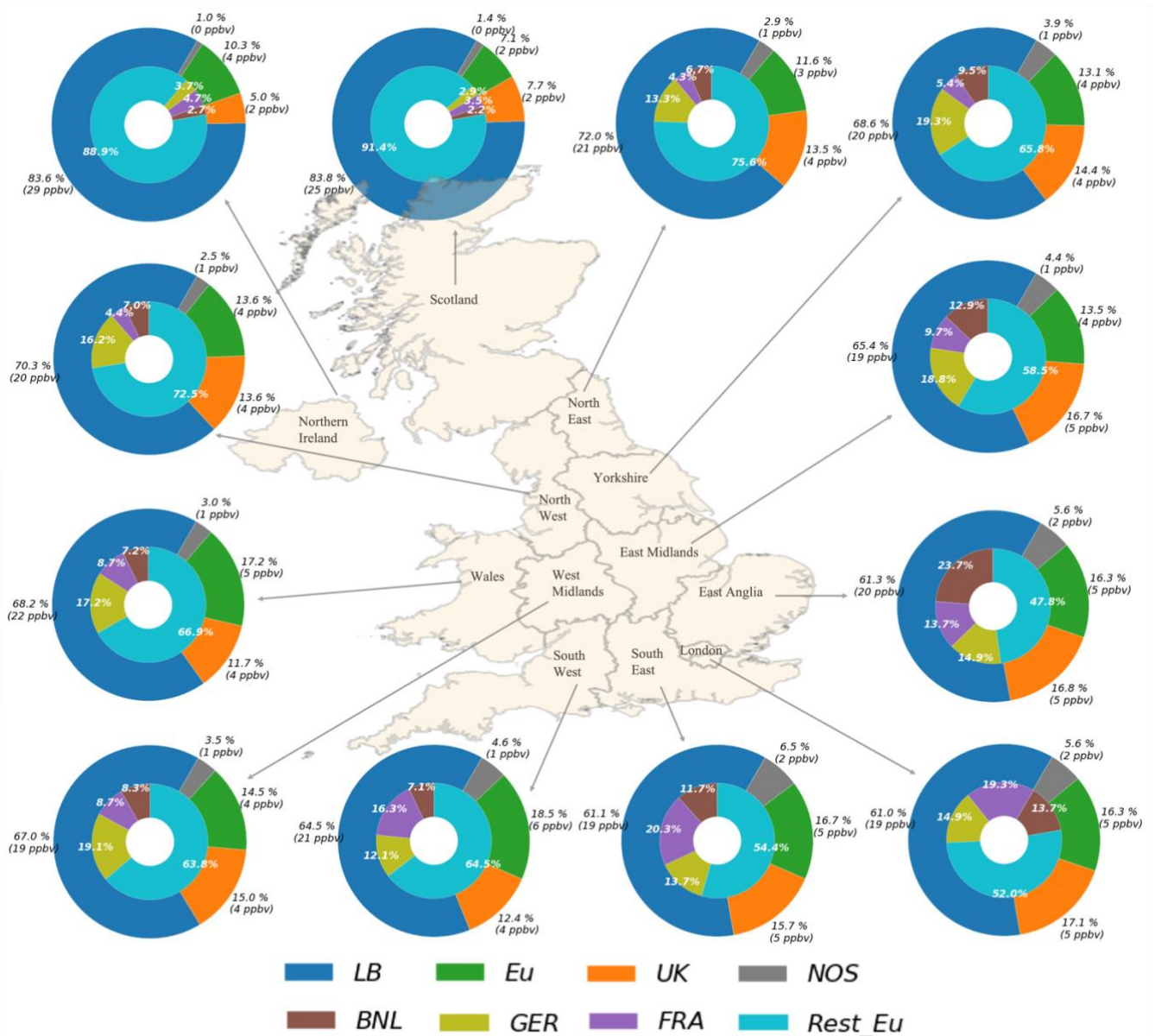


Figure S10. Simulated contributions to the mean O₃ mixing ratios in June 2015 over 12 receptor regions in the UK. Outer circle depicts the contributions from LB, UK, Eu super-region (Eu), and the NOS. The inner circle breaks down the contribution from the Eu super-region into four sub-regions: The Benelux (BNL), France (FRA), Germany (GER), and the rest of Europe (Rest_Eu). Note that the values correspond to the contributions from anthropogenic sources only, with the exception of the LB which includes O₃ from stratospheric origin.

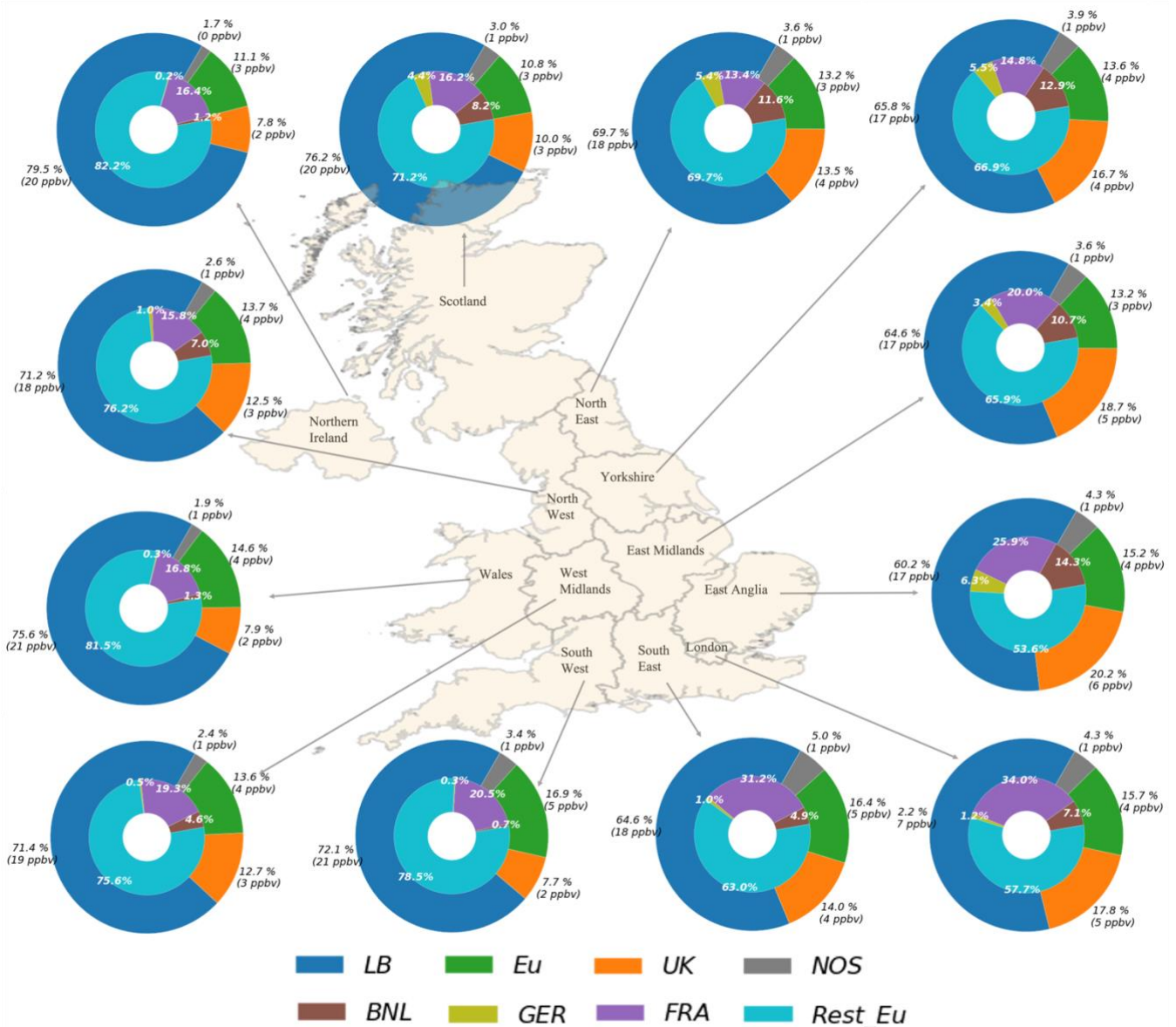


Figure S11. Simulated contributions to the mean O₃ mixing ratios in July 2015 over 12 receptors regions in the UK. Outer circle depicts the contributions from LB, UK, Eu super-region (Eu), and the NOS. The inner circle breaks down the contribution from the Eu super-region into four sub-regions: The Benelux (BNL), France (FRA), Germany (GER), and the rest of Europe (Rest_Eu). Note that the values correspond to the contributions from anthropogenic sources only, with the exception of the LB which includes O₃ from stratospheric origin.

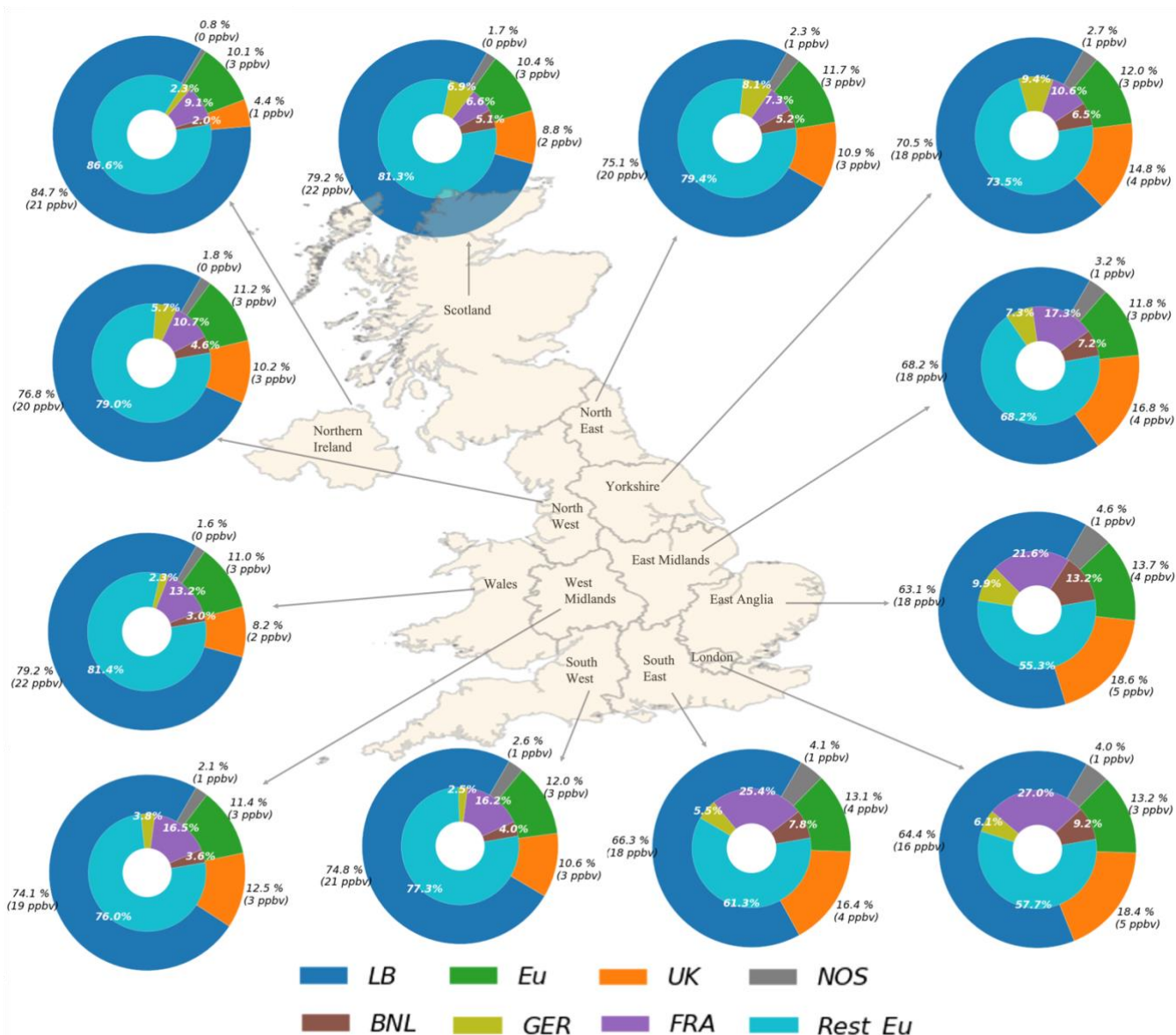


Figure S12. Simulated contributions to the mean O₃ mixing ratios in August 2015 over 12 receptors regions in the UK. Outer circle depicts the contributions from LB, UK, Eu super-region (Eu), and the NOS. The inner circle breaks down the contribution from the Eu super-region into four sub-regions: The Benelux (BNL), France (FRA), Germany (GER), and the rest of Europe (Rest_Eu). Note that the values correspond to the contributions from anthropogenic sources only, with the exception of the LB which includes O₃ from stratospheric origin.

References

- Archer-Nicholls, S., Lowe, D., Utembe, S., Allan, J., Zaveri, R. A., Fast, J. D., & Hodnebrog, Ø.: Gaseous chemistry and aerosol mechanism developments for version 3.5.1 of the online regional model, WRF-Chem, *Geosci. Model Dev.*, 7, 2557–2579. <https://doi.org/10.5194/gmd-7-2557-2014>, 2014
- Carslaw, D. C., & Ropkins, K.: Openair - An R package for air quality data analysis. *Environ. Model. Softw.*, 27–28, 52–61. <https://doi.org/10.1016/j.envsoft.2011.09.008>, 2012
- Crilly, L.; Kramer, L.; Reed, C.; Lee, J.D.; Massey-Woodward, R.; Whalley, L., Forster, G.; Bandy, B.: ICOZA: Atmospheric species measurements of OH, HONO, HO₂, NO, NO₂, NO_y, O₃, SO₂ and CO from Weybourne Atmosphere Observatory July 2015. Centre for Environmental Data Analysis [data set]. <http://catalogue.ceda.ac.uk/uuid/ddf1032d626b45f78ce1c5e94f289a66>, 2018
- Francis, X. V., Chemel, C., Sokhi, R. S., Norton, E. G., Ricketts, H. M. A., & Fisher, B. E. A.: Mechanisms responsible for the build-up of ozone over South East England during the August 2003 heatwave. *Atmos. Environ.*, 45(38), 6880–6890. <https://doi.org/10.1016/j.atmosenv.2011.04.035>, 2011
- Gao, M., Han, Z., Liu, Z., Li, M., Xin, J., Tao, Z., Li, J., Kang, J.-E., Huang, K., Dong, X., Zhuang, B., Li, S., Ge, B., Wu, Q., Cheng, Y., Wang, Y., Lee, H.-J., Kim, C.-H., Fu, J. S., Wang, T., Chin, M., Woo, J.-H., Zhang, Q., Wang, Z., and Carmichael, G. R.: Air quality and climate change, Topic 3 of the Model Inter-Comparison Study for Asia Phase III (MICS-Asia III) –Part1: Overview and model evaluation, *Atmos. Chem. Phys.*, 18, 4859–4884, <https://doi.org/10.5194/acp-18-4859-2018>, 2018
- Knote, C., Tuccella, P., Curci, G., Emmons, L., Orlando, J. J., Madronich, S., Baró, R., Jiménez-Guerrero, P., Luecken, D., Hogrefe, C., Forkel, R., Werhahn, J., Hirtl, M., Pérez, J. L., San José, R., Giordano, L., Brunner, D., Yahya, K., & Zhang, Y.: Influence of the choice of gas-phase mechanism on predictions of key gaseous pollutants during the AQMEII phase-2 intercomparison. *Atmos. Environ.*, 115, 553–568. <https://doi.org/10.1016/j.atmosenv.2014.11.066>, 2014
- Mar, K. A., Ojha, N., Pozzer, A., & Butler, T. M.: Ozone air quality simulations with WRF-Chem (v3.5.1) over Europe: Model evaluation and chemical mechanism comparison, *Geosci. Model Dev.*, 9(10), 3699–3728. <https://doi.org/10.5194/gmd-9-3699-2016>, 2016
- Met Office: Met Office integrated data archive system (MIDAS) land and marine surface stations data [data set]. <http://catalogue.ceda.ac.uk/uuid/916ac4bbc46f7685ae9a5e10451bae7>, 2006
- Tao, Z., Chin, M., Gao, M., Kucsera, T., Kim, D., Bian, H., Kurokawa, J., Wang, Y., Liu, Z., Carmichael, G. R., Wang, Z., and Akimoto, H.: Evaluation of NU-WRF model performance on air quality simulation under various model resolutions –an investigation within the framework of MICS-Asia PhaseIII, *Atmos. Chem. Phys.*, 20, 2319–2339, <https://doi.org/10.5194/acp-20-2319-2020>, 2020
- Tørseth, K., Aas, W., Breivik, K., Fjæraa, A. M., Fiebig, M., Hjellbrekke, A. G., Lund Myhre, C., Solberg, S., & Yttri, K. E.: Introduction to the European Monitoring and Evaluation Programme (EMEP) and observed atmospheric composition change during 1972-2009. *Atmos. Chem. Phys.*, 12(12), 5447–5481. <https://doi.org/10.5194/acp-12-5447-2012>, 2012
- Zhao, C., Huang, M., Fast, J. D., Berg, L. K., Qian, Y., Guenther, A., Gu, D., Shrivastava, M., Liu, Y., Walters, S., Pfister, G., Jin, J., Shilling, J. E., and Warneke, C.: Sensitivity of biogenic volatile organic compounds to land surface parameterizations and vegetation distributions in California, *Geosci. Model Dev.*, 9, 1959–1976, <https://doi.org/10.5194/gmd-9-1959-2016>, 2016
- Zhang, Y., Sartelet, K., Zhu, S., Wang, W., Wu, S. Y., Zhang, X., Wang, K., Tran, P., Seigneur, C., & Wang, X. F.: Application of WRF / Chem-MADRID and WRF / Polyphemus in Europe – Part 2 : Evaluation of chemical concentrations and sensitivity simulations., *Atmos. Chem. Phys.*, 6845–6875. <https://doi.org/10.5194/acp-13-6845-2013>, 2013